ACS APPLIED MATERIALS & INTERFACES

Research Article

www.acsami.org

A Silica–Gold–Silica Nanocomposite for Photothermal Therapy in the Near-Infrared Region

Song Liang,[†,§] Yang Zhao,[†] Shuping Xu,[†] Xu Wu,[†] Jiao Chen,[†] Min Wu,[‡] and Julia Xiaojun Zhao*[,†]

[†]Department of Chemistry and [‡]Department of Biochemistry and Molecular Biology, University of North Dakota, Grand Forks, North Dakota 58202, United States

[§]Key Laboratory of Bionic Engineering (Ministry of Education), College of Biological and Agricultural Engineering, Jilin University, Changchun 130022, China

ABSTRACT: The focus of this work was to study the photothermal effect of a silica–gold–silica nanocomposite in the near-infrared (NIR) region. The NIR region is considered a biological window because living cells and tissues have low light scattering and adsorption in this region. Both a laser source and a tungsten lamp source were used in this study. The critical parameters for photothermal efficiency, including nancomposite concentration and irradiation time, were evaluated. The penetration of the nanocomposites into mammalian cells was also investigated. With laser irradiation, the nanocomposite showed a significant photothermal effect in the NIR region. The maximal temperature that the nanocomposites could reach was 51.9 °C. Vybrant assays showed that 5 min of laser irradiation along with the nanocomposite caused target cell death through both apoptosis (59%) and necrosis (31%), while controls showed minimal effects. The nanocomposite may be a potential light-absorbing agent for NIR fluorescence-guided photothermal therapy.

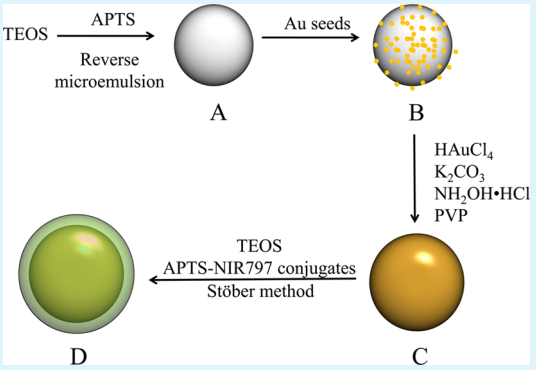

KEYWORDS: *photothermal therapy, near-infrared, fluorescence, gold nanoshell*

1. INTRODUCTION

Nanomaterials have demonstrated a broad range of applications in the field of biological and biomedical studies including biosensing,[1,2] bioimaging,[3−5] drug delivery,[6,7] cancer diagnosis,[8−10] cancer therapy,[11−13] etc. The combination of multiple functions into one nanoparticle has generated a number of new multifunctional nanomaterials for bioapplications.[13−15] A typical example is a nanoparticle coupled with bioimaging and controlled drug delivery functions. Usually, the bioimaging ability of a multifunctional nanoparticle is fulfilled via encapsulation of MRI contrast agents[14,16,17] or fluorophores[17] into the nanoparticle. The controlled drug delivery can be realized by photoinduced hyperthermia[18−22] or drug release.[7,12,13] Therefore, a multiple functional nanoparticle can specifically deliver drugs to a tumor site under the guidance of biosensing reagents.

Recently, applications of multifunctional nanoparticles have been extended to various photoinduced therapies such as photodynamic therapy, photomechanical therapy, and photothermal therapy. Among these therapeutic methods, photothermal therapy is a convenient and promising technique for killing tumor cells because of its high efficiency and limited invasiveness. The laser-induced photothermal therapy can selectively destroy tumor cells via localized hyperthermia.

In conventional photothermal therapy, a photoabsorbing agent is needed to convert the energy of radiation to heat. Traditional photosensitive molecules are not good candidates as photoabsorbing agents because of their limitation of stability and absorption of radiation. In the past decade, to overcome these limitations, nanomaterials with large absorption cross sections and good photostability have been developed and applied to photothermal therapy, including noble metal nanostructures and carbon nanotubes.

Noble metal nanostructures, especially gold nanostructures, have garnered great interest for photothermal therapy because of their strong absorption abilities, tunable extinction spectra, and ease of surface modification.[22,23] Most common gold nanostructures, such as gold nanospheres,[24] gold nanorods,[25,26] gold nanoshells,[18,17−31] and gold nanocages,[32,33] can be used as photoabsorbing agents for photothermal therapy. Although the optical properties of these gold nanostructures are different, their absorption cross sections are a few orders of magnitude higher than those of the molecular dyes.[24] The absorption and scattering efficiency of the gold nanostructures can be manipulated by changing their morphology. Because of their unique photoabsorbing ability, various gold-based nanoparticles have been used to develop multifunctional nanoparticles for use in photothermal therapy.[19,20,34]

In spite of the broad applications discussed above, the gold-based nanomaterials have not been fully applied to photothermal therapy under the guidance of fluorescence imaging in

Received: October 29, 2013
Accepted: December 3, 2014
Published: December 3, 2014

the near-infrared (NIR) region. The NIR region is considered a biological window because living cells and tissues have low light scattering and adsorption in this region. NIR fluorescence has been widely applied for biosensing and imaging.[19,25] The NIR region is also suitable for gold nanomaterials to absorb light and convert it to heat. Thus, the purpose of this work was to demonstrate a potential of gold nanomaterial-based nanocomposite for photothermal therapy in the NIR region. The nanocomposite was developed by doping two components, NIR dye molecules and gold nanostructures, into a silica nanomatrix. This nanoparticle can penetrate cells through an endocytosis process. The cells can be imaged using a relatively weak NIR irradiation. Furthermore, guided by the fluorescence images, the laser-induced photothermal therapy can kill target cells in a localized area with minimum damage to adjacent cells and tissues. Finally, if the excitation wavelength of the NIR fluorescence material overlaps the absorption band of the gold nanostructures, a single energy-adjustable laser source can be applied for both NIR fluorescence sensing and photothermal therapy.

2. EXPERIMENTAL SECTION

Chemicals and Instruments. NIR-797 isothiocyanate (less than 70%), gold(III) chloride trihydrate ($HAuCl_4$, 99.9+%), polyvinylpyrrolidone (PVP, average molecular weight = 10 000), dimethyl sulfoxide (DMSO, 99.9%, ACS reagent), and hydroxylamine hydrochloride (98%, ACS grade) were purchased from Sigma-Aldrich Co. Tetraethyl orthosilicate (TEOS, 98%, ACS grade) and sodium borohyride (98+%) were purchased from Acros Organics. Cyclohexane (HPLC grade) and potassium carbonate anhydrous (ACS grade) were obtained from Fischer Scientific. *n*-Hexanol (99%, ACS grade) and Triton X-100 were purchased from Alfa Aesar. Ammonium hydroxide (28−30%, GR grade) was purchased from EM Industries Inc. A Vybrant apoptosis/necrosis assay kit (YO-PRO-1 dye and propidium iodide) was purchased from Invitrogen Co. A serum-free medium (Roswell Park Memorial Institute (RPMI) 1640 with *l*-glutamine) was purchased from Mediatech Inc. Herndon. The phosphate-buffered saline (PBS) tablets were ordered from MP Biomedicals LLC. A mouse alveolar macrophage cell line (MH-S) was purchased from ATCC. Ultra-purified water (18.3 MΩ cm) used in all experiments was obtained using a Milli-Q Millipore water purification system.

A Shimadzu UV-250 PC UV−vis spectrophotometer was used to measure the absorbance of samples. A Jobin Yvon Horiba Fluorolog-3 spectrofluorometer with a NIR detector was employed for fluorescence measurements. A Hitachi 7500 transmission electron microscope was used to obtain the transmission electron microscopy (TEM) images of the synthesized nanoparticles. A Carl Zeiss LSM 510 Meta laser scanning confocal microscope with a warming plate (Carl Zeiss MicroImaging, Inc.) was used to investigate the apoptosis and necrosis of the macrophage cells. An Olympus 1 × 71 fluorescence microscope was used to take NIR fluorescence images (exciter, HQ775/50; emitter, HQ845/55; beam splitter, Q810 long pass). An Eppendorf 5804 centrifuge was used for separation of silica nanoparticles from solutions. A BWF1 series fiber-coupled diode laser system (450 mW at 808 nm) from B&W TEK Inc. was used for the photothermal effect study. A SK-1250MC electronic thermometer was purchased from Sato Keiryoki MFG. CO., Ltd.

Synthesis of the Gold Nanocomposite. The silica−gold−silica nanocomposite was synthesized using our previous reported method[35] based on a modified literature method.[36] Gold nanoseeds were attached on the surface of an amine-functionalized silica core. A gold layer then grew on the core from the gold seeds. A silica shell containing NIR-797 was coated on the SiO_2−Au core−shell nanostructure using a Stöber method.

Synthesis of Control Silica Nanoparticles. The Stöber method was employed to synthesize the control silica nanoparticles. A reaction mixture was made by adding 0.54 mL of H_2O, 0.50 mL of TEOS, and 1.00 mL of 28−30% ammonium hydroxide to 12.80 mL of ethanol. This mixture was continuously stirred for 24 h and then washed three times with ethanol. The prepared nanoparticles were dispersed in 40.0 mL of water for future use.

Temperature Measurements for Nanocomposite Solutions. Two light sources were used to irradiate the nanocomposite solutions: a 450 mW fiber-coupled NIR diode laser and a 100 W tungsten lamp. An electronic thermometer was employed to monitor the temperature. The lab-made experimental setup is shown in Figure 1. The output end of the laser was placed against a 1 cm^2 plastic cuvette. When the tungsten lamp was in use, the light was focused on a small area of 1.0 mL of solution in a glass cylindrical cuvette. To minimize the heat loss, the cuvette was sealed by a rubber stopper and covered with asbestos cloth. During the measurement, the sensor tip of the thermometer is inserted in the cell culture dish in Figure 1. To account for the potential nonuniform temperature, the solutions were continuously stirred during the irradiation. The temperature was measured at different time intervals.

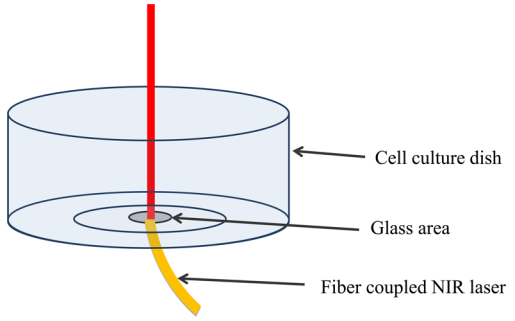

Figure 1. Experimental setup for photothermal detection of targeting cells using a NIR laser.

Penetration of Nanocomposite into Macrophage Cells. MH-S cells were cultured on glass-bottomed plates with a serum-free medium at 37 °C in a 5% CO_2 and humidified atmosphere overnight. A 1.6 mg/mL nanocomposite solution was diluted by 10-fold using the serum-free medium. After removal of the culture medium, 200 μL of 0.16 mg/mL nanocomposite solution was added to each plate. These cells were incubated for certain periods of time (1, 2, and 4 h). The cells were then observed under a fluorescence microscope.

Study of Photothermal Effect of Nanocomposites. The cell culture was carried out as described in the previous section. After 2 h of incubation with the nanocomposite, the culture medium with nanocomposite was removed. The cells in each dish were gently washed with 200 μL of PBS buffer. A 1.0 mL aliquot of serum-free medium was then added to the dish. The cells were treated using a fiber-coupled diode NIR laser for 5−30 min. The power density of the laser at 808 nm was estimated to be about 0.57 W/cm^2, and the divergence angle of the laser beam out of the fiber was about 27°. The output end of the laser was perpendicularly placed just below the glass part of the culture dish. The treatment area was marked before irradiation. During laser treatment, the cells remained in the incubator at 37 °C with 5% CO_2 in a humidified atmosphere. The control samples were prepared using control silica nanoparticles instead of the nanocomposite.

Vybrant Assay. A 10.0 μL aliquot of 0.1 μM YO-PRO-1 and 0.1 μg/mL propidium iodide was added to the samples. After 5 min of staining, the samples were observed under a confocal fluorescence microscope with a 40× objective lens at 37 °C. An argon laser was used as a light source for the apoptosis study. The corresponding emission filter was a 505−550 nm band-pass filter. A helium−neon laser was used as a light source for the necrosis study. The corresponding emission filter was a 580 nm long pass filter. The percentages of apoptotic and necrotic cells were calculated based on the corresponding cell numbers.

3. RESULTS AND DISCUSSION

The Nanocomposites. On the basis of the literature work, gold nanostructures are good candidates for photothermal materials.[36,38] Under NIR irradiation, gold nanomaterials can absorb electromagnetic energy and convert it to thermal energy. Usually, the absorption of the pure gold nanospheres is in the visible range.[36] However, a silica–gold core–shell nanoparticle may have a strong absorption in the NIR region.[12] When a gold layer is coated on the silica nanoparticle, the gold plasmon band shifts to a longer wavelength. The extent of this wavelength shift depends on the thickness of the gold shell and the size of the silica core. A suitable size of the silica core was selected based on the previous work (Figure 2A).[5,39] To form

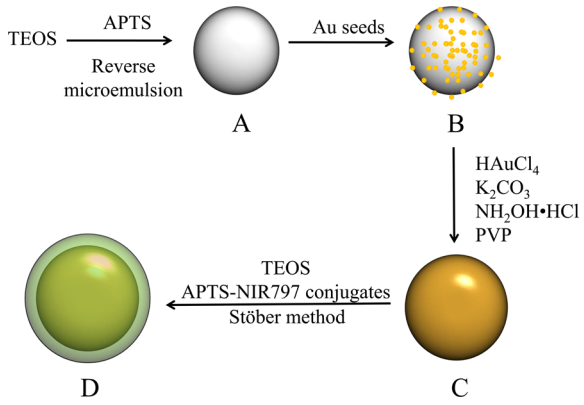

Figure 2. Schematic diagram of fabrication of the nanocomposite. (A) A silica core. (B) Au seeds adsorbed on the silica core. (C) A gold shell was formed on the silica core. (D) Silica outer containing NIR dye molecules were formed to complete the formation of the nanocomposite.

the gold layer, the gold colloid seeds were first physically adsorbed onto the surface of an amine-functionalized silica nanoparticle (Figure 2B). In a gold growth solution, the seeds grew to a thin gold shell (Figure 2C). To fulfill the goal of detection of targets, NIR dye molecules were incorporated into the nanoparticle. The NIR-797 was first conjugated with (3-aminopropyl)triethoxysilane (APTES) through the covalent conjugation before being doped into the silica layer. Then, the outer silica layer containing NIR-797 was directly formed onto the gold layer by cohydrolization of TEOS and NIR-797–APTES (Figure 2D). The NIR-797 was distributed in the outer silica shell associated with APTES. It has been reported that the absorption of pulsed laser light energy at the plasmon resonant wavelength of silica–gold core–shell nanoparticles could result in a reshaping of the nanoparticle's metal shell layer, which might change the absorption properties despite being beneficial for lasting effects.[40,41] Thus, besides hosting dye molecules, the outer silica could protect the gold layer from morphology change due to the rigidity of the silica shell.

Characterization. The optical properties of the gold nanostructures greatly depend on their size, shape, and core–shell composition.[23,24,35,37] The thickness and internal and outer diameters of a gold shell affect its extinction spectrum.[35,36] The TEM images showed that the average size of the silica core was 140 ± 20 nm in diameter (Figure 3A). The average size of the SiO_2–Au core–shell nanoparticles was 170 ± 30 nm in diameter (Figure 3B). Therefore, the thickness of the gold layer was about 15 nm. After being coated with the outer silica, the final size of the nanoparticles was 240 ± 20 nm (Figure 3C).

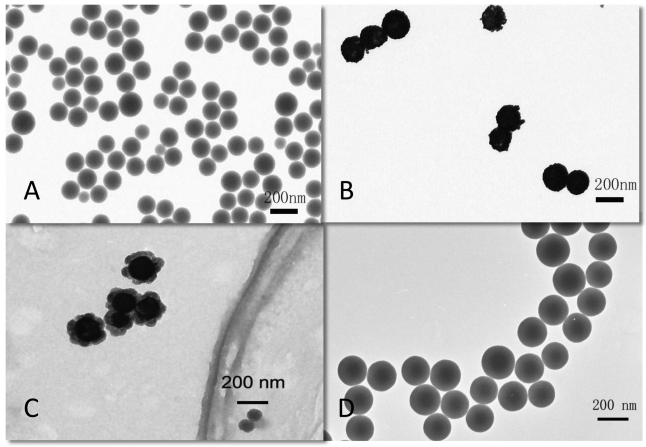

Figure 3. TEM images of the nanocomposites and control nanoparticles. (A) Silica cores (140 ± 20 nm); (B) SiO_2–Au core–shell nanoparticles (170 ± 30 nm); (C) SiO_2–Au–SiO_2 nanocomposites (240 ± 20 nm); (D) control silica nanoparticles without gold layer (221 ± 17 nm).

Pure silica nanoparticles without any dopants were prepared as the control nanoparticles. A Stöber method was used to obtain the uniform control nanoparticles.[42] TEM images showed that the average size of the control nanoparticles was 221 ± 17 nm in diameter (Figure 3D). The size of a control nanoparticle was comparable to that of a nanocomposite.

The absorption spectra showed that the extinction band of gold seeds was in the visible range (Figure 4A, curve a), while the nanocomposite had a broad extinction band in the NIR region (Figure 4A, curve b). A broad extinction peak is a typical property of gold nanoshells, which might also suggest the nonuniformity of the thickness of the gold layer.[36,37] The strong extinction in the NIR region endowed the nanocomposite with the intended photothermal therapy capability. The broad extinction peak allowed a relatively large wavelength range for selection of a suitable irradiation source. Meanwhile, the nanocomposites could convert a broad range of NIR light to thermal energy to increase the photothermal efficiency when a continuous light source was used. In this work, both a laser source and a continuous irradiation source were employed.

In a bulk solution, NIR-797 can be excited at 760 nm, which shows two emission peaks within 780–1000 nm (Figure 4B, curve a). When the NIR-797 was doped in the nanocomposites, its emission spectrum changed slightly with a small red-shift (Figure 4B, curve b). The red-shift is a common phenomenon for doped fluorophores, which might suggest the existence of dye aggregates in the nanomatrix.[36,37]

Photothermal Effect Using a Laser as an Irradiation Source. To test the photothermal effect of the nanocomposites, a 450 mW diode laser with an emission wavelength of 808 nm was used to irradiate the nanocomposites. The initial results indicated that two major factors influenced the photothermal effect. One was the irradiation time, and the other was the concentration of the nanocomposites. Thus, these two factors were studied in detail. The temperatures of the nanoparticle solutions under irradiation were monitored in situ using a thermal probe. The same volume of pure water was used as a control.

The concentrations of the nanocomposites were varied from 0.05–0.80 mg/mL. After irradiation for 30 min, the temperature of pure water increased slightly from (25.1 ± 0.1) °C to

dx.doi.org/10.1021/am507644b | ACS Appl. Mater. Interfaces 2015, 7, 85–93

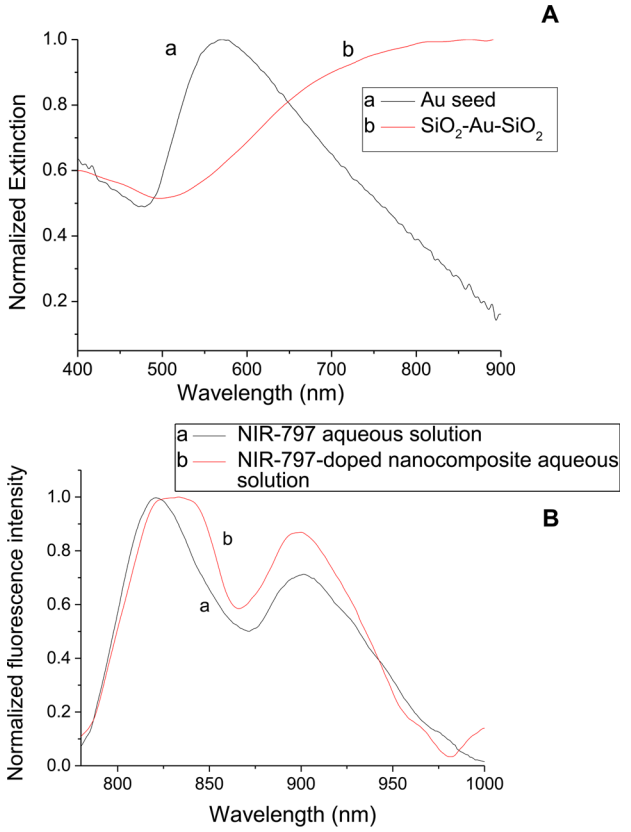

Figure 4. (A) Normalized extinction spectra of 87.0 μg/mL gold seeds (curve a) and 0.80 mg/mL nanocomposites (curve b). (B) Normalized fluorescence spectra of 0.01 mg/mL NIR-797 aqueous solution (curve a) and 0.80 mg/mL NIR-797 doped SiO_2–Au–SiO_2 nanocomposite aqueous solution (curve b). The excitation wavelength was 760 nm, pH = 7.4.

(27.4 ± 0.1) °C (Figure 5A, curve a). In contrast, a 1.0 mL aliquot of 0.05 mg/mL nanocomposite solution showed a significant change in temperature. A total of 11.8 °C increase was obtained by this nanocomposite solution (Figure 5A, curve b). When the concentration of the nanoparticles was increased to 0.10 mg/mL, an additional 4.6 °C of increase was achieved (Figure 5A, curve c). The 0.30 mg/mL nanoparticle solution showed the highest photothermal effect in which the temperature reached 51.9 °C (Figure 5A, curve e). Beyond this threshold, the continuous increase of the concentration of the nanocomposite showed no obvious changes in temperature (Figure 5A, curves f and g). This result indicated that 0.30 mg/mL nanocomposite is the optimal concentration to generate the highest temperature. There might be two reasons for the appearance of this optimal concentration. First, the incident intensities of the laser and the tungsten lamp are not very large in the absorb band of nanocomposites. Even if the concentration of the nanocomposites increased to a higher concentration, there is not enough photons to be absorbed. Therefore, the further increase of nanocomposite concentration higher than a certain threshold would no longer contribute to the temperature increase of a solution. Second, the plateau phase to a temperature curve might indicate that the system reached thermal equilibrium. The increase of solution temperature enlarged the temperature difference between the solution and outer environment, which enhanced the heat transfer. Therefore, the heat loss continued to increase as the solution

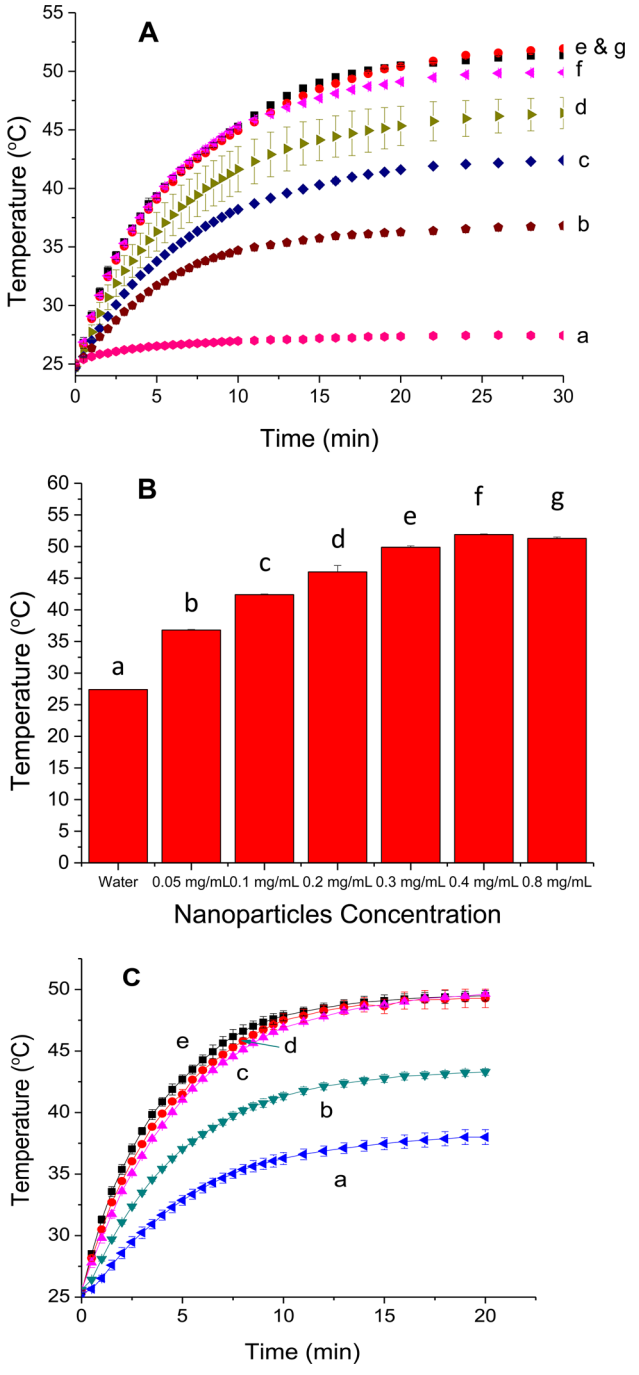

Figure 5. (A) Temperature measurements with various nanocomposite concentrations. Light source: a 450 mW diode NIR laser. Nanocomposite concentration: (a) 0 mg/mL (water); (b) 0.05 mg/mL; (c) 0.10 mg/mL; (d) 0.20 mg/mL; (e) 0.30 mg/mL; (f) 0.40 mg/mL; (g) 0.80 mg/mL. (B) Average temperature change for nanocomposite solutions in the first 10 min. Light source: a 450 mW diode NIR laser. Nanocomposite concentration: (a) 0 mg/mL (water); (b) 0.05 mg/mL; (c) 0.10 mg/mL; (d) 0.20 mg/mL; (e) 0.30 mg/mL; (f) 0.40 mg/mL; (g) 0.80 mg/mL. (C) Temperature measurements with various nanocomposite concentrations. Light source: a 100 W tungsten lamp. Nanocomposite concentration: (a) 0.10 mg/mL; (b) 0.20 mg/mL; (c) 0.40 mg/mL; (d) 0.80 mg/mL; (e) 1.60 mg/mL.

temperature increased until the heat loss balanced the heat generation. Thus, the thermal equilibrium was reached, and temperature was almost constant. In either case, the optimal nanocomposite concentration for this study was 0.30 mg/mL.

dx.doi.org/10.1021/am507644b | ACS Appl. Mater. Interfaces 2015, 7, 85−93

The concentration of nanocomposites played an important role in the photothermal effect. The temperature increase was comparable to the reported photothermal materials.[42] Since the hyperthermia in the temperature higher than 43 °C could selectively destroy malignant cells,[43] the prepared nanoparticles can be a new type of effective photothermal material for killing malignant cells.

The irradiation time influenced the photothermal effect as well. Regardless of the concentrations of nanoparticles, the solutions showed very similar results in which the temperature increased rapidly in the first 10 min (Figure 5A). Then, the temperature increase rate slowed down in the remaining time. Finally, when the irradiation time was extended to 30 min, the solutions reached thermal equilibrium. The temperature was stabilized at the maximum temperature. As shown in Figure 5, panel B, the highest temperature under irradiation was related to the concentration of the nanocomposites. The higher the nanocomposite concentration was, the higher the temperature would be reached. When the nanocomposite concentration increased to 0.30 mg/mL, the temperature increase reached the maximum value. If the nanocomposite concentration was higher than 0.30 mg/mL, the maximum temperature remained relatively constant even if the nanoparticle concentration increased (Figure 5B, columns e−g).

It should be noted that the laser only heated the limited volume in its pathway. If the laser beam was ideally narrowed, the heated volume was only 0.03% of the total volume. This heated volume was calculated by multiplying the light path with the cross section of the beam. Although only a very small portion of the solution was irradiated by the laser, the solution temperature increased by about 27.0 °C above room temperature. If the laser is used for a localized photothermal treatment, the temperature increase in the treated small volume should be even higher.

Photothermal Effect Using a Lamp as an Irradiation Source. To compare the photothermal effect of different irradiation sources, a 100 W tungsten lamp was used as the light source for the heating study. Similarly, varied concentrations of the nanoparticle solution were tested after different irradiation periods of time. The results showed that nanocomposite solution had a similar temperature increase trend to the solution when a laser was used (Figure 5C). A higher concentration of the nanocomposite resulted in a higher temperature increase. However, the final temperatures were slightly lower than those irradiated by the laser. The highest temperature was about 49.6 °C in contrast to 51.9 °C by the laser. In fact, the tungsten lamp irradiated a much larger volume of solution than did the laser. The reason for the lower temperature increase might be due to the broad wavelength range of the tungsten lamp. The highest absorbance of the SiO_2−Au−SiO_2 nanocomposite was located in the NIR region (Figure 4A), which led to the decrease in energy transfer efficiency when the broad wavelength light source was used. However, if a desired laser source is not available, the tungsten lamp could provide a moderate photothermal effect.

Penetration of the Nanocomposite into Living Cells. To apply the nanocomposite to photothermal therapy, the penetration of the nanocomposites into living cells was investigated. An effective penetration was the foundation for this application. The effectiveness includes the penetration time and the amount of penetrated nanoparticles. Mouse alveolar macrophage MH-S cells were selected for this study as these cells are a great model to evaluate the lung macrophages in clearing invading

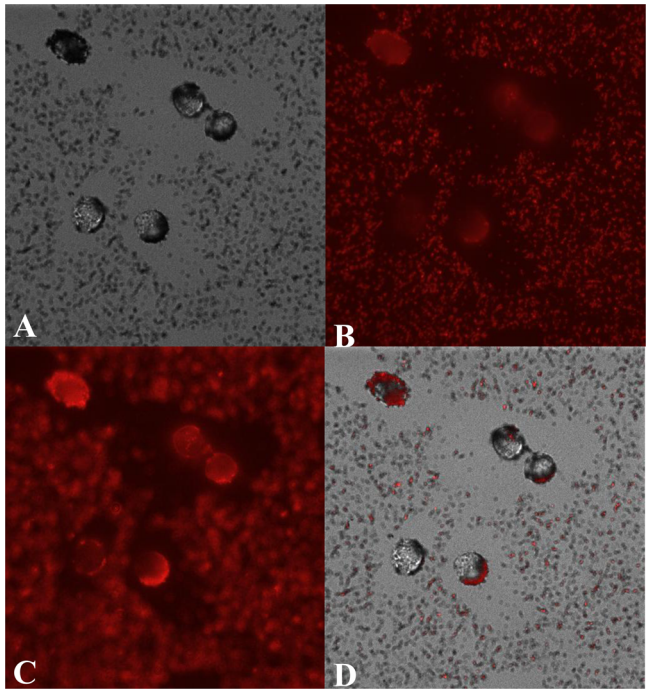

Figure 6. Fluorescence and bright field images of endocytosis of nanocomposites into MH-S cells at 2 h. (A) Bright field image; (B) fluorescence image focused on the nanocomposites outside the cells; (C) fluorescence image focused on the nanocomposites inside the cells; (D) bright light and fluorescence merged image.

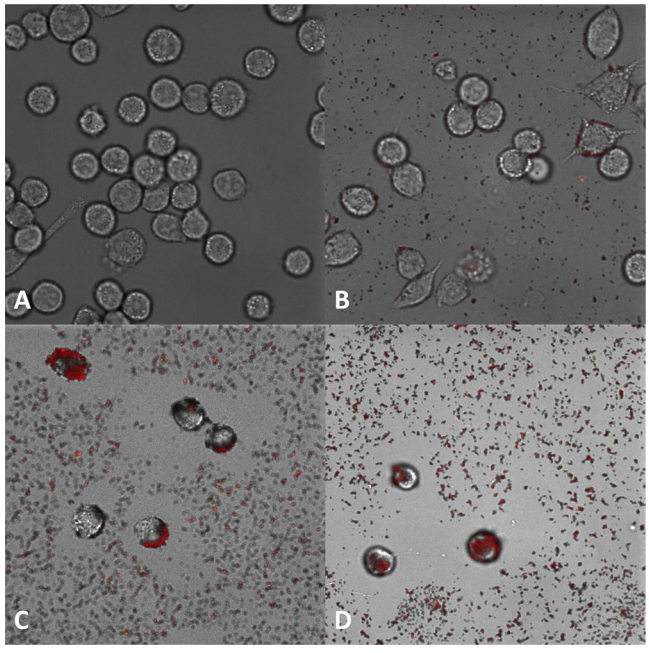

Figure 7. Merged images of MH-S cells incubated with nanocomposites for different times. (A) 0 h without nanocomposites; (B) 1 h; (C) 2 h; (D) 4 h. The merged images show the bright field images and the corresponding fluorescence image.

macromolecules. To trace the nanoparticle movement, the fluorescence images were taken using the NIR fluorescence from doped NIR-797.

The endocytosis of the nanocomposites into the MH-S cells was monitored using a fluorescence microscope. Both bright field images and fluorescence images were taken after 2 h of

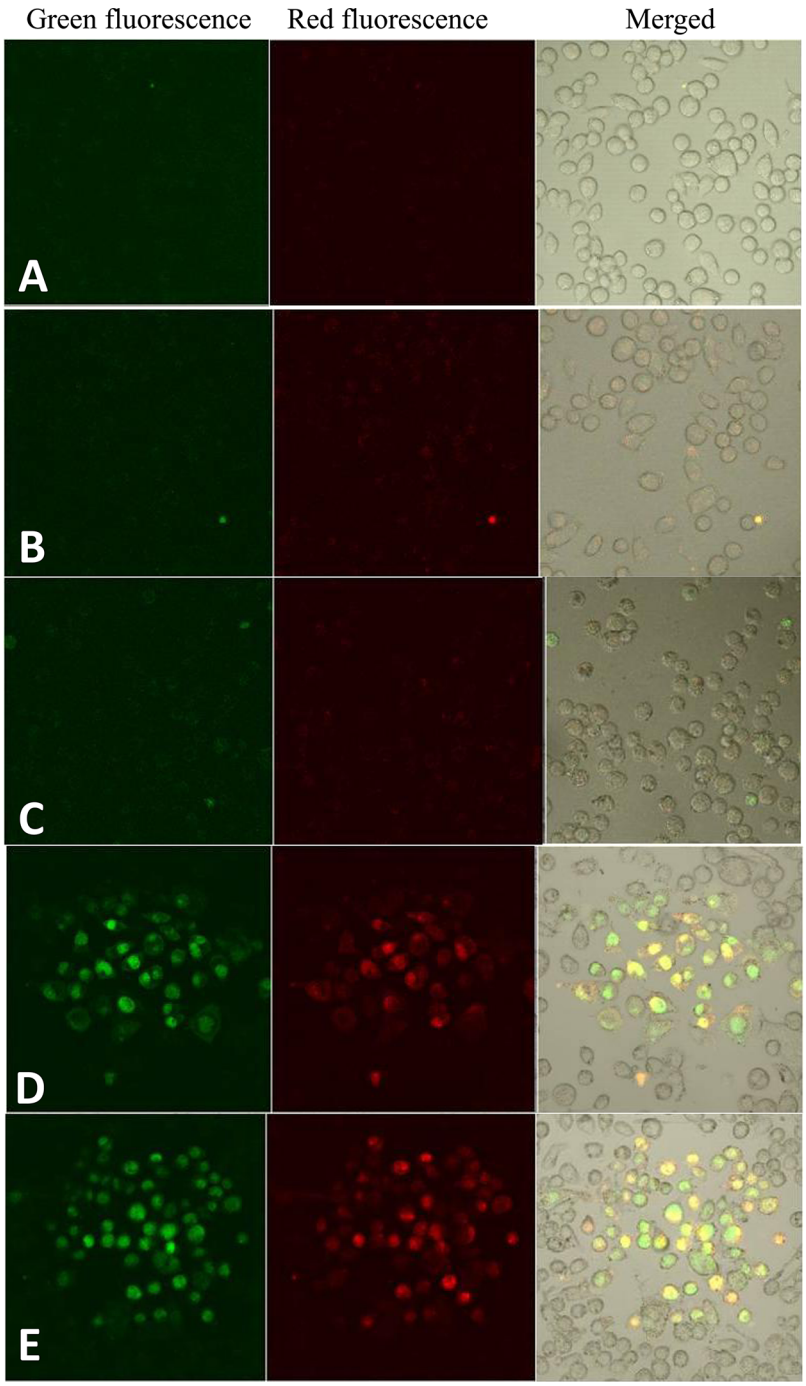

Figure 8. Vybrant assay using a confocal fluorescence microscope. (A) MH-S cells without nanoparticles or laser treatment; (B) MH-S cells incubated with the control nanoparticles for 2 h, irradiation time = 5 min; (C) MH-S cells incubated with the nanocomposites for 2 h, irradiation time = 0 min; (D) MH-S cells incubated with the nanocomposites for 2 h, irradiation time = 5 min; (E) MH-S cells incubated with the nanocomposites for 2 h, irradiation time = 30 min. Green stain represents the apoptotic cells; red fluorescence represents the necrotic cells; the merged image combines the fluorescence images and the corresponding bright field image.

incubation. The images clearly showed that a large number of nanocomposites penetrated the cells. In a bright field image, some nanocomposite adsorbed onto the glass substrate and appeared as black dots (Figure 6A). In the same image, the MH-S cells showed some dark areas as well, which represented the nanocomposites that penetrated the cells or absorbed on their surface. In the corresponding fluorescence image, the nanocomposites exhibited strong NIR fluorescence (Figure 6B,C). The nanoparticles uptaken by cells and those adsorbed on the glass substrate could be distinguished by adjusting the focus distance when the fluorescence images are taken. In Figure 6, panel B, the nanocomposites on the glass substrate were focused. The nanocomposites were clearly observed, while the fluorescence from the nanocomposites inside the cells was dim and blurry. Figure 6, panel C showed that the nanocomposites on the substrate were out of focus, and the cells were in focus. The fluorescence inside the cells turned bright, and the image of some nanocomposites in the cells became sharp and clear. This result indicated that the nanocomposites entered into the MH-S cells. More evidence for the penetration of the

dx.doi.org/10.1021/am507644b | ACS Appl. Mater. Interfaces 2015, 7, 85−93

nanocomposites into the MH-S cells was that few nanocomposites were found in the area surrounding the cells. This phenomenon indicated that the MH-S cells had ingested the nanoparticles from the nearby area through phagpcytosis.

The penetration of nanocomposites into MH-S cells depends on the particle size. It has been confirmed that the larger the particle size, the longer the time for penetration.[18] In this work, we only chose one size of nanoparticles. The uptake time of this nanoparticle into the cells was investigated using a fluorescence microscope. After MH-S cells were incubated with the fluorescent nanocomposites, time-lapse images were taken. As shown in Figure 7, panel A, before the nanocomposites were added, the MH-S cells were healthy. After incubation with the nanocomposites for 1 h, some MH-S cells with "branches" were observed under the microscope. These branches were pseudopods, through which MH-S cells can ingest the nanocomposites (Figure 7B). Meanwhile, the majority of the nanocomposites in the image were adsorbed to the glass substrate, while only a few nanocomposites had penetrated the cells. As the incubation time reached 2 h, more nanoparticles appeared in the cells (Figure 7C). Few nanoparticles could be found on the glass substrate near the cells. When the incubation time increased to 4 h, the phenomenon was similar to that of the 2 h incubation (Figure 7D). Thus, the 2 h incubation time was selected for the penetration of the nanocomposites.

In Vitro Photothermal Treatment of Macrophage Cells Using the Nanocomposites. The nanocomposites exhibited strong photothermal capability. To further explore their potential as photothermal therapy materials, Vybrant assay was employed. The assay examined whether the photothermal effect of the nanoparticles could effectively kill target cells. In the Vybrant assay, a green dye, YO-PRO-1, was used to stain the apoptotic cells, while a red dye, propidium iodide, was used to stain the necrotic cells. Therefore, when the photothermal effect caused cell death through apoptotic pathway, the cell would appear in a green color. However, if the cell died through the necrotic route, the red color would appear.

A few controls were used in these investigations. The first control was pure MH-S cells without any irradiation or nanoparticle treatments. The results showed no stained cells in the fluorescence image (Figure 8A). The MH-S cells in this sample were assumed healthy. Control two was the pure silica nanoparticles without gold shell and NIR-797 doping. After 5 min of laser irradiation, fluorescence images were taken. Few colored spots appeared in the image (Figure 8B). The number of dead cells was not significant. The results indicated that the pure silica nanoparticles without gold shell were not toxic to cells with irradiation. In control three, the cells were cultured with the nanocomposites without irradiation (Figure 8C). Slightly stained cells were found in control three. The toxicity of the nanocomposites was not significant. The result concurred with the literature work.[44]

Under the same conditions, the cells cultured with the nanocomposites were placed under a laser irradiation for 5 min. A significant amount of cell death was observed (Figure 8D). Both green and red colors appeared, which indicates that the photothermal effect killed cells through both necrosis and apoptosis. As the irradiation continued to 30 min, more cell deaths were observed (Figure 8E). The image clearly shows that the cells located in a round area were killed, while the cells out of this area were still alive.

Overall, the large number of stained cells in the laser-treated area suggests an effective laser-induced photothermal effect. By contrast, the neighboring cells showed no apparent staining. The results have demonstrated that the photothermal effect of the nanoparticles could focus on the targeting area without damage of nontarget area cells.

The percentage of apoptotic and necrotic cells was determined by counting the numbers of green cells and red cells. The cell death in controls one and two could be ignored. Control three showed 3−4% cell death. In the presence of the nanocomposites, we noted that apoptotic cells were 59 ± 8%, while the necrotic cells were 31 ± 7% after 5 min of laser irradiation. When the laser irradiation time increased to 30 min, the percentage of apoptotic and necrotic cells also increased to 65% and 35%, respectively. The results showed that the photothermal effect of nanoparticles may effectively kill the target cells.

4. CONCLUSIONS

In summary, the SiO_2−Au−SiO_2 nanocomposites demonstrated a broad extinction in the NIR region, which showed a significant photothermal effect in the solution. Irradiated by a 450 mW NIR laser, the temperature of a 0.3 mg/mL nanocomposite solution could be increased from room temperature (25 °C) to 51.9 °C within 30 min. If a tungsten lamp was employed as the irradiation source, a slightly lower temperature increase was observed. The nanocomposites could penetrate MH-S cells within 2 h. The potential of the nanocomposites as photothermal therapy materials was explored in vitro. Vybrant assay showed that 5 min of laser irradiation could cause cell death (59 ± 8% apoptotic, while 31 ± 7% necrotic). When the irradiation time increased to 30 min, the percentage of apoptotic and necrotic cells increased to (65 ± 7)% and (35 ± 20)%, respectively. Compared to the literature, the significant features of our design are the absorption in the NIR region and the usage of a low power laser. Doping NIR-797 dye molecules in the outer silica, the nanocomposites can be used for fluorescence sensing in the NIR region. Since the excitation wavelength of NIR-797 is close to the extinction band of the gold nanospheres, this method has the potential to develop a relatively simple device for sensing and treatment with a single light source. The low power laser is adequate to generate high temperatures required for killing tumor cells. Therefore, the nanocomposites have a great potential as light-absorbing agents for photothermal therapy.

AUTHOR INFORMATION

Corresponding Author

*E-mail: jzhao@chem.und.edu. Phone: 701-777-3610. Fax: 701-777-2331.

Notes

The authors declare no competing financial interest.

ACKNOWLEDGMENTS

This work was supported by the USA National Science Foundation Grants No. CHE 0911472, CHE 0947043, ND EPSCoR through NSF Grant No. IIA-1355466, and the Neuroscience COBRE Pilot Grant through the University of North Dakota.

REFERENCES

(1) Xu, P.; Yu, H.; Li, X. Functionalized Mesoporous Silica for Microgravimetric Sensing of Trace Chemical Vapors. *Anal. Chem.* **2011**, *83*, 3448−3454.

(2) Au, L.; Zheng, D.; Zhou, F.; Li, Z.; Li, X.; Xia, Y. A Quantuative Study on the Photothermal Effect of Immuno Gold Nanocages Targeted to Breast Cancer Cells. *ACS Nano* **2008**, *2*, 1645−1652.
(3) Buck, S. M.; Lee, Y. K.; Park, E.; Xu, H.; Philbert, M. A.; Brasuel, M. A.; Kopelman, R. Optochemical Nanosensor PEBBLEs: Photonic Explorers for Bioanalysis with Biologically Localized Embedding. *Curr. Opin. Chem. Biol.* **2004**, *8*, 540−546.
(4) Chen, J.; Wang, D.; Xi, J.; Au, L.; Siekkinen, A.; Warsen, A.; Li, Z.; Zhang, H.; Xia, Y.; Li, X. Immuno Gold Nanocages with Tailored Optical Properties for Targeted Photothermal Destruction of Cancer Cells. *Nano Lett.* **2007**, *7*, 1318−1322.
(5) Song, J.; Zhang, W.; Miao, K.; Zeng, H.; Cheng, S.; Fan, L. Receptor-Free Poly(phenylenevinylene) Fibrous Membranes from Cation Sensing: High Sensitivity and Good Selectivity Achieved by Choosing the Appropriate Polymer Matrix. *ACS Appl. Mater. Interfaces* **2013**, *5*, 4011−4016.
(6) del Monte, F.; Levy, D. Formation of Fluorescent Rhodamine B J-Dimers in Sol-Gel Glasses Induced by the Adsorption Geometry on the Silica Surface. *J. Phys. Chem. B* **1998**, *102*, 8036−8041.
(7) Ferrer, M. L.; del Monte, F.; Levy, D. Rhodamine 19 Fluorescent Dimers Resulting from Dye Aggregation on the Porous Surface of Sol-Gel Silica Glasses. *Langmuir* **2003**, *19*, 2782−2786.
(8) Rajesh, S.; Funston, A. M.; Mulvaney, P.; Murray, R. W. Gold Nanoparticles: Past, Present, and Future. *Langmuir* **2009**, *25*, 13840−13851.
(9) Gobin, A. M.; Lee, M. H.; Halas, N. J.; James, W. D.; Drezek, R. A.; West, J. L. Near-Infrared Resonant Nanoshells for Combined Optical Imaging and Photothermal Cancer Therapy. *Nano Lett.* **2007**, *7*, 1929−1934.
(10) Heitsch, A. T.; Smith, D. K.; Patel, R. N.; Ress, D.; Korgel, B. A. Multifunctional Particles: Magnetic Nanocrystals and Gold Nanorods Coated with Fluorescent Dye-Doped Silica Shells. *J. Solid State Chem.* **2008**, *181*, 1590−1599.
(11) Sengupta, S.; Kulkarni, A. Design Principles for Clinical Efficacy of Cancer Nanomedicine: A Look into the Basics. *ACS Nano* **2013**, *7*, 2878−2882.
(12) Hirsch, L. R.; Stafford, R. J.; Bankson, J. A.; Sershen, S. R.; Rivera, B.; Price, R. E.; Hazle, J. D.; Halas, N. J.; West, J. L. Nanoshell-Mediated Near-Infrared Thermal Therapy of Tumors under Magnetic Resonance Guidance. *Proc. Natl. Acad. Sci. U.S.A.* **2003**, *100*, 13549−13554.
(13) Huang, X.; El-Sayed, I. H.; Qian, W.; El-Sayed, M. A. Cancer Cell Imaging and Photothermal Therapy in the Near-Infrared Region by Using Gold Nanorods. *J. Am. Chem. Soc.* **2006**, *128*, 2115−2120.
(14) Huang, X.; Jain, P.; El-Sayed, I. H.; El-Sayed, M. A. Plasmonic Photothermal Therapy (PPTT) Using Gold Nanoparticles. *Laser. Med. Sci.* **2008**, *23*, 217−228.
(15) Jain, P. K.; Lee, K. S.; El-Sayed, I. H.; El-Sayed, M. A. Calculated Absorption and Scattering Properties of Gold Nanoparticles of Different Size, Shape, and Composition: Applications in Biological Imaging and Biomedicine. *J. Phys. Chem. B* **2006**, *110*, 7238−7248.
(16) Ji, X.; Shao, R.; Elliott, A. M.; Stafford, J.; Esparza-Coss, E.; Bankson, J. A.; Liang, G.; Luo, Z.; Park, K.; Markert, J. T.; Li, C. Bifunctional Gold Nanoshells with a Superparamagnetic Iron Oxide−Silica Core Suitable for Both MR Imaging and Photothermal Therapy. *J. Phys. Chem. C* **2007**, *111*, 6245−6251.
(17) Rejinold N, S.; Chennazhi, K. P.; Tamura, H.; Nair, S. V.; Jayakumar, R. Multifunctional Chitin Nanogels for Simultaneous Drug Delivery, Bioimaging, and Biosensing. *ACS Appl. Mater. Interfaces* **2011**, *3*, 3654−3665.
(18) Jin, Y.; Lohstreter, S.; Pierce, D. T.; Parisien, J.; Wu, M.; Hall, C.; Zhao, J. X. Silica Nanoparticles with Continuously Tunable Sizes: Synthesis and Size Effects on Cellular Contrast Imaging. *Chem. Mater.* **2008**, *20*, 4411−4419.
(19) Kawano, T.; Niidome, Y.; Mori, T.; Katayama, Y.; Niidome, T. PNIPAM Gel-Coated Gold Nanorods for Targeted Delivery Responding to a Near-Infrared Laser. *Bioconjugate Chem.* **2009**, *20*, 209−212.
(20) Kim, J.; Kim, H. S.; Lee, N.; Kim, T.; Kim, H.; Yu, T.; Song, I. C.; Moon, W. K.; Hyeon, T. Multifunctional Uniform Nanoparticles Composed of a Magnetite Nanocrystal Core and a Mesoporous Silica Shell for Magnetic Resonance and Fluorescence Imaging and for Drug Delivery. *Angew. Chem., Int. Ed.* **2008**, *47*, 8438−8441.
(21) Kim, S.; Ohulchanskyy, T. Y.; Pudavar, H. E.; Pandey, R. K.; Prasad, P. N. Organically Modified Silica Nanoparticles Co-Encapsulating Photosensitizing Drug and Aggregation-Enhanced Two-Photon Absorbing Fluorescent Dye Aggregates for Two-Photon Photodynamic Therapy. *J. Am. Chem. Soc.* **2007**, *129*, 2669−2675.
(22) Larson, D. R.; Zipfel, W. R.; Williams, R. M.; Clark, S. W.; Bruchez, M. P.; Wise, F. W.; Webb, W. W. Water-Soluble Quantum Dots for Multiphoton Fluorescence Imaging in Vivo. *Science* **2003**, *300*, 1434−1436.
(23) Larson, T. A.; Bankson, J.; Aaron, J.; Sokolov, K. Hybrid Plasmonic Magnetic Nanoparticles as Molecular Specific Agents for Mri/Optical Imaging and Photothermal Therapy of Cancer Cells. *Nanotechnology* **2007**, *18*, 325101.
(24) Lin, Y.; Haynes, C. L. Impacts of Mesoporous Silica Nanoparticle Size, Pore Ordering, and Pore Integrity on Hemolytic Activity. *J. Am. Chem. Soc.* **2010**, *132*, 4834−4842.
(25) Liong, M.; Lu, J.; Kovochich, M.; Xia, T.; Ruehm, S. G.; Nel, A. E.; Tamanoi, F.; Zink, J. I. Multifunctional Inorganic Nanoparticles for Imaging, Targeting, and Drug Delivery. *ACS Nano* **2008**, *2*, 889−896.
(26) Liu, H.; Wu, S.; Lu, C.; Yao, M.; Hsiao, J.; Hung, Y.; Lin, Y.; Mou, C.; Yang, C.; Huang, D.; Chen, Y. Mesoporous Silica Nanoparticles Improved Magnetic Labeling Efficiency in Human Stem Cells. *Small* **2008**, *4*, 619−626.
(27) Liu, S.; Liang, Z. S.; Gao, F.; Luo, S. F.; Lu, G. Q. In Vitro Photothermal Study of Gold Nanoshells Functionalized with Small Targeting Peptides to Liver Cancer Cells. *J. Mater. Sci. Mater. Med.* **2010**, *21*, 665−674.
(28) Loo, C.; Lowery, A.; Halas, N.; West, J.; Drezek, R. Immunotargeted Nanoshells for Integrated Cancer Imaging and Therapy. *Nano Lett.* **2005**, *5*, 709−711.
(29) Norman, R. S.; Stone, J. W.; Gole, A.; Murphy, C. J.; Sabo-Attwood, T. L. Targeted Photothermal Lysis of the Pathogenic Bacteria, *Pseudomonas aeruginosa*, with Gold Nanorods. *Nano Lett.* **2008**, *8*, 302−306.
(30) O'Neal, D. P.; Hirsch, L. R.; Halas, N. J.; Payne, J. D.; West, J. L. Photothermal Tumor Ablation in Mice Using Near Infrared-Absorbing Nanoparticles. *Cancer Lett.* **2004**, *209*, 171−176.
(31) Ohulchanskyy, T. Y.; Roy, I.; Goswami, L. N.; Chen, Y.; Bergey, E. L.; Pandey, R. K.; Oseroff, A. R.; Prasad, P. N. Organically Modified Silica Nanoparticles with Covalently Incorporated Photosensitizer for Photodynamic Therapy of Cancer. *Nano Lett.* **2007**, *7*, 2835−2842.
(32) Overgaard, J. Effect of Hyperthermia on Malignant Cells in Vivo: A Review and a Hypothesis. *Cancer* **1977**, *39*, 2637−2646.
(33) Pérez-Justea, J.; Pastoriza-Santosa, I.; Liz-Marzána, L. M.; Mulvaneyb, P. Gold Nanorods: Synthesis, Characterization, and Applications. *Coord. Chem. Rev.* **2005**, *249*, 1870−1901.
(34) Qian, H. S.; Guo, H. C.; Ho, P. C.; Mahendran, R.; Zhang, Y. Mesoporous-Silica-Coated Up-Conversion Fluorescent Nanoparticles for Photodynamic Therapy. *Small* **2009**, *5*, 2285−2290.
(35) Xu, S.; Hartvickson, S.; Zhao, J. Z. Engineering of SiO_2−Au−SiO_2 Sandwich Nanoaggregates Using a Building Block: Single, Double, and Triple Cores for Enhancement of Near-Infrared Fluorescence. *Langmuir* **2008**, *24*, 7492−7499.
(36) Radloff, C.; Halas, N. J. Enhanced Thermal Stability of Silica-Encapsulated Metal Nanoshells. *Appl. Phys. Lett.* **2001**, *79*, 674−677.
(37) Santra, S.; Zhang, P.; Wang, K.; Tapec, R.; Tan, W. Conjugation of Biomolecules with Luminophore-Doped Silica Nanoparticles for Photostable Biomarkers. *Anal. Chem.* **2001**, *73*, 4988−4993.
(38) Sharma, P.; Brown, S. C.; Singh, A.; Iwakuma, N.; Pyrgiotakis, G.; Krishna, V.; Knapik, J. A.; Barr, K.; Moudgil, B. M.; Grobmyer, S. R. Near-Infrared Absorbing and Luminescent Gold Speckled Silica Nanoparticles for Photothermal Therapy. *J. Mater. Chem.* **2010**, *20*, 5182−5185.

(39) Slowing, I. I.; Trewyn, B. G.; Giri, S.; Lin, V. S. Mesoporous Silica Nanoparticles for Drug Delivery and Biosensing Applications. *Adv. Funct. Mater.* **2007**, *17*, 1225−1236.
(40) Slowing, I. I.; Vivero-Escoto, J. L.; Wu, C.; Lin, V. S. Mesoporous Silica Nanoparticles as Controlled Release Drug Delivery and Gene Transfection Carriers. *Adv. Drug Delivery Rev.* **2008**, *60*, 1278−1288.
(41) Aguirre, C. M.; Moran, C. E.; Yound, J. F.; Halas, N. J. Laser-Induced Reshaping of Metallodielectric Nanoshells under Femtosecond and Nanosecond Plasmon Resonant Illumination. *J. Phys. Chem. B* **2004**, *108*, 7040−7045.
(42) Smith, J. E.; Medley, C. D.; Tang, Z.; Shangguan, D.; Lofton, C.; Tan, W. Aptamer-Conjugated Nanoparticles for the Collection and Detection of Multiple Cancer Cells. *Anal. Chem.* **2007**, *79*, 3075−3082.
(43) Dewey, W. C. Arrhenius Relationships from the Molecule and Cell to the Clinic. *Int. J. Hyperthermia* **2009**, *25*, 3−20.
(44) Jin, Y.; Kannan, S.; Wu, M.; Zhao, J. X. Toxicity of Luminescent Silica Nanoparticles to Living Cells. *Chem. Res. Toxicol.* **2007**, *20*, 1126−1133.